Validation of an organ mapping antibody panel for cyclical immunofluorescence microscopy on normal human kidneys

Brewer, Maya; Migas, Lukasz G.; Clouthier, Kelly A.; Allen, Jamie L.; Anderson, David M.; Pingry, Ellie; Farrow, Melissa; Quardokus, Ellen M.; Spraggins, Jeffrey M.; Van de Plas, Raf

DOI
10.1152/ajprenal.00426.2023

Publication date
2024

Document Version
Final published version

Published in
American journal of physiology. Renal physiology

AMERICAN JOURNAL OF PHYSIOLOGY
RENAL PHYSIOLOGY

Am J Physiol Renal Physiol 327: F91–F102, 2024.
First published May 9, 2024; doi:10.1152/ajprenal.00426.2023

RESEARCH ARTICLE

Validation of an organ mapping antibody panel for cyclical immunofluorescence microscopy on normal human kidneys

Maya Brewer,[1]* Lukasz G. Migas,[2]* Kelly A. Clouthier,[1] Jamie L. Allen,[3,4] David M. Anderson,[3,5] Ellie Pingry,[3,4] Melissa Farrow,[3,5] Ellen M. Quardokus,[6] Jeffrey M. Spraggins,[3,4,5,7,8] Raf Van de Plas,[2,3,5] and Mark P. de Caestecker[1,4]

[1]*Division of Nephrology, Department of Medicine, Vanderbilt University Medical Center, Nashville, Tennessee, United States;* [2]*Delft Center for Systems and Control, Delft University of Technology, Delft, The Netherlands;* [3]*Mass Spectrometry Research Center, Vanderbilt University School of Medicine, Nashville, Tennessee, United States;* [4]*Department of Cell and Developmental Biology, Vanderbilt University School of Medicine, Nashville, Tennessee, United States;* [5]*Department of Biochemistry, Vanderbilt University School of Medicine, Nashville, Tennessee, United States;* [6]*Department of Intelligent Systems Engineering, Indiana University, Bloomington, Indiana, United States;* [7]*Department of Chemistry, Vanderbilt University School of Medicine, Nashville, Tennessee, United States; and* [8]*Department of Pathology, Microbiology and Immunology, Vanderbilt University Medical Center, Nashville, Tennessee, United States*

Abstract

The lack of standardization in antibody validation remains a major contributor to irreproducibility of human research. To address this, we have applied a standardized approach to validate a panel of antibodies to identify 18 major cell types and 5 extracellular matrix compartments in the human kidney by immunofluorescence (IF) microscopy. We have used these to generate an organ mapping antibody panel for two-dimensional (2-D) and three-dimensional (3-D) cyclical IF (CyCIF) to provide a more detailed method for evaluating tissue segmentation and volumes using a larger panel of markers than would normally be possible using standard fluorescence microscopy. CyCIF also makes it possible to perform multiplexed IF microscopy of whole slide images, which is a distinct advantage over other multiplexed imaging technologies that are applicable to limited fields of view. This enables a broader view of cell distributions across larger anatomical regions, allowing a better chance to capture localized regions of dysfunction in diseased tissues. These methods are broadly accessible to any laboratory with a fluorescence microscope, enabling spatial cellular phenotyping in normal and disease states. We also provide a detailed solution for image alignment between CyCIF cycles that can be used by investigators to perform these studies without programming experience using open-sourced software. This ability to perform multiplexed imaging without specialized instrumentation or computational skills opens the door to integration with more highly dimensional molecular imaging modalities such as spatial transcriptomics and imaging mass spectrometry, enabling the discovery of molecular markers of specific cell types, and how these are altered in disease.

NEW & NOTEWORTHY We describe here validation criteria used to define on organ mapping panel of antibodies that can be used to define 18 cell types and five extracellular matrix compartments using cyclical immunofluorescence (CyCIF) microscopy. As CyCIF does not require specialized instrumentation, and image registration required to assemble CyCIF images can be performed by any laboratory without specialized computational skills, this technology is accessible to any laboratory with access to a fluorescence microscope and digital scanner.

antibody; cyclical immunofluorescence; human; kidney; validation

INTRODUCTION

Despite global efforts over the past 15 years to improve standards for antibody validation (1–5), the lack of standardization in antibody validation and use remains a major contributor to irreproducibility of research (6, 7). This has been of particular concern with immunohistochemical staining studies since even minor differences in tissue preparation and preservation techniques can have significant effects on both nonspecific staining and true antibody cross-reactivities (8). The emergence of multidisciplinary consortia that are using a wide range of technologies to map cellular characteristics at a single cell level in human tissues (9) has further increased our dependence on the use of validated antibodies as true anchors of cell registration to integrate these diverse datasets within the intact tissue architecture

*M. Brewer and L. G. Migas contributed equally to this work.
Correspondence: M. P. de Caestecker (mark.de.caestecker@vumc.org).
Submitted 2 January 2024 / Revised 11 March 2024 / Accepted 26 March 2024

(10–12). These studies include the use of antibodies labeled with a variety of different conjugates for a range of different multiplexed immunofluorescence (MxIF) techniques, including DNA-conjugated antibodies used for co-detection by indexing (CODEX) (13, 14), fluorescently conjugated antibodies used for cyclic immunofluorescence (CyCIF) (15), and iterative bleaching extends multiplicity (IBEX) (16), as well as the use of rare earth metal isotope-conjugated antibodies used for imaging mass cytometry (IMC) (17). These techniques allow us to generate composite images of tissues stained simultaneously with large numbers of antibodies (with up to 60 markers using CODEX[13]), enabling accurate cell identification and segmentation, and determination of changes in cell states in health and disease. However, without proper validation of each antibody used under the conditions of the respective assays, including antibody conjugation, tissue processing, and staining and destaining protocols, the data input may be perturbed by incorrectly presenting antibody-based data points that may have unforeseen effects on subsequent analyses of these highly dimensional datasets.

To address these challenges, the Human BioMolecular Atlas Program (HuBMAP) (18, 19) has developed guidelines for antibody validation for MxIF applications. For this, a series of organ mapping antibody panels (OMAPs) are being developed supported by documentation of antibody characteristics, validation criteria, and tissue preparation protocols. These are incorporated into antibody validation reports (AVRs) on the HuBMAP website (https://avr.hubmapconsortium.org/), with supporting imaging data located on a public database (https://zenodo.org/communities/omap?q=&l=list&p=1&s=10&sort=newest) (20). OMAPs are integrated into the Anatomical Structures, Cell Types plus Biomarkers (ASCT + B) Tables (https://humanatlas.io/asctb-tables) and visualized in the ASCT + B Reporter (https://humanatlas.io/asctb-reporter) to support tissue mapping efforts across consortia (21).

As part of the Vanderbilt Biomolecular Imaging Center, one of the Tissue Mapping Centers (TMC) in the HuBMAP consortium (18, 19), our laboratory has been performing CyCIF on frozen tissue sections obtained from discarded tumor-adjacent normal human kidney specimens from patients with renal cancer undergoing nephrectomy (22, 23). For these studies, CyCIF imaging is being used to provide cell identification and segmentation by integrating fluorescence signals from validated antibodies, with multimodal imaging of sequential sections using spatially targeted multiomics assays including imaging mass spectrometry (IMS) (24, 25). Similar integration of data from different antibody-based imaging modalities with spatial transcriptomics and single cell multiomics sequencing is being performed to enhance the spatial resolution of these RNA and DNA-based datasets in normal and diseased human kidneys by other participants in the HuBMAP and Kidney Precision Medicine Program (KPMP) Consortia, respectively (18, 19, 26). However, unlike other multiplex imaging techniques, such as CODEX, CyCIF can be performed at scale on large numbers of sections with large surface areas of tissue without specialized instrumentation or analytical tools (15). In this paper, we describe and have applied modifications of antibody validation criteria that have been used by other laboratories specifically for immunohistochemical validation on human tissue samples (5, 27), specifically for the use of a panel of 27 different antibodies and a lectin to define the major cell types and extra cellular matrix compartments on frozen adult human kidney sections. We go onto validate the use of 17 of these antibodies and one lectin to define the major tubular and glomerular cell types and associated structures in a series of 2-D and 3-D CyCIF imaging studies.

MATERIALS AND METHODS

Tissue Collection and Preparation

Deidentified human kidney samples were obtained from disease-free tumor-associated nephrectomy samples after removal of pathology specimens by the Vanderbilt Cooperative Human Tissue Network (CHTN, IRB Protocols No. 181822 "Biomolecular Multimodal Imaging for 3-Dimensional Tissue Mapping of the Human Kidney"). Deidentified information including the patient's HuBMAP identification number (deidentified), age, sex, ethnicity, reason for surgery, and diagnosis are included in the Supplemental Tables S1, S2, and S3 for the different experiments. Samples were collected on ice within 1–2 h of surgery. Tissue blocks (~0.5 cm × 1 cm × 2–4 cm) were cut, extending from the cortex through the medulla on their long axis, and frozen in 2.6% carboxymethylcellulose (CMC; Fischer, No. C9481) in water, or 2% low melting point gelatin (LMG) on a dry ice/isopentane slurry (Sigma, No. 03551-4) and stored at −80°C prior to sectioning (23).

Immunofluorescence Staining

Ten-micrometer sections from CMC-mounted tissue blocks and 8-μm sections from LMG-mounted tissue blocks were cut onto Superfrost Plus slides (Fisher, No. 12-550-15), refrozen at −80°C, and postfixed in 10% neutral-buffered formalin (Sigma, No. HT501128) for 5 min at room temperature (RT), washed with phosphate-buffered saline (PBS) at the time of staining. We did not subject the sections to antigen retrieval, as previously described (23). Sections were demarcated using a hydrophobic pen (Vector Laboratories, No. H-4000) and placed in a humidified chamber for staining. Slides were initially incubated for 5 min with 50 mM glycine in PBS (Sigma, No. 410225) to reduce autofluorescence, followed by blocking for 30 min at RT in Universal Blocking Reagent (UBR, Biogenex, No. HK085-5K). Primary antibodies were incubated overnight at 4°C in Antibody Diluent Reagent (ADR, Fisher, No. 003218) and washed three times with PBS. For indirect immunofluorescence (IF), slides were incubated with fluorophore-conjugated secondary antibodies for 60 min at RT and washed again three times in PBS. All primary and secondary antibodies, dilutions, and fluorophores used are indicated in Table 1 and Supplemental Tables S1, S2, and S3. Some antibodies were detected by indirect IF, as indicated, while others were either purchased or conjugated in-house with the indicated fluorophores, as previously described (28). Sections were then incubated with Hoechst 33342 (Fisher, No. 62249) at 1:5,000 of a 20 mM solution in PBS for 10 min, washed twice in PBS, and mounted in 50% glycerol/PBS (Fisher, No. G33) before coverslipping. Slides were stored in a humidified chamber at 4°C until imaging was performed. Digital images were scanned using a Zeiss AxioScan Z1 slide scanner with a ×10 objective (Carl Zeiss Microscopy, Oberkochen, Germany).

Table 1. *Antibodies validated for immunofluorescence microscopy on frozen human kidneys*

Target	Cell Types	Company	Cat. No.	Clone ID	Species	Conjugate	Conj Test	Antibody Costaining	Supplemental Figs.	Validate Criteria	CyCIF Cycles
THP/UMOD	TAL	R&D	AF5144	PC	Sheep	UC	NT	THP, CALB1, KRT8, ZO1, NaKATP, NCC	13, 24, 25, 26	3	1, 4
THP/UMOD	TAL	Alpha	J65429#	PC	Rabbit	UC	NT	THP	24	3	NT
Nestin (NES)	Pods (cyto)	Novus	NB300-266 + AF488	10C2	Mouse	UC, AF488 (C)	Yes	PODXL, SYNPO, Tensin, COL4A5	9, 16	2, 1	1
Laminin g1 (LAMC1)	GBM, TBM, BV, GN caps	DHSB	2E8	2E8	Mouse	AF488 (IH)	Yes	LAMC1, COL4A12, CD31, PODXL, COL4A5, aSMA, TNS1	5, 7, 8, 10, 14, 18, 23	3, 2, 1	NT
Laminin g1 (LAMC1)	GBM, all TBMs, vessel walls, GN caps	DHSB	D18	D18	Mouse	UC	NT	LAMC1 (2E8)	14	3	NT
Podocalyxin (PODXL)	Podocyte (cyto, PM)	Abcam	AB211225 AB208254	EPR9518	Rabbit	AF568, AF488 (C)	Yes	SYNPO, NES, LAMC1, CD31	16, 16, 18	2	2
Zona occludens-1 (ZO1)	Podocyte and TAL PM >DTL, ATL, DCT, CNT, CD	TF	TF-61-7300	PC	Rabbit	AF594 (IH)	Yes	AQP1, AQP2, THP, SYNPO, TNS1	25, 26, 27, 28	2, 1	4
CD93	All ECs	Sigma	HPA009300	PC	Rabbit	UC	NT	CD31	4	2	NT
CD31/PECAM	All ECs	Abcam	AB215912	JC/70A	Mouse	AF647 (C)	Yes	CD93, LAMC1, PODXL, aSMA, WT1 SYNPO	4, 5, 18, 21, 22	2, 1	2
Collagen IV a1/2 (Col4A1/2)	TBM, MM, GN-cap, PT-ECM	TF	53-9871-82 AF488/647	1042	Mouse	AF488, AF647 (C)	Yes	COL4A12, LAMC1, TNS1, SYNPO, COL4A5	6, 7, 10	3, 1	4
Collagen IV a1/2 (Col4A1/2)	TBM, MM, GN-cap, PT-ECM	Millipore	MAB3326	IV-4H12	Mouse	UC AF488 (IH)	Yes	COL4A12, LAMC1	6, 8	3	NT
Aquaporin 1 (AQP1)	PTECs-S1, S2, S3	Santa Cruz	SC-25287 + AF488	H4	Mouse	UC, AF488 (C)	Yes	AQP1, LTL, ZO1, SLC5A12, SGLT2, LRP2, AQP2, KRT8	1, 12, 15, 19, 20	3	2, 3
Aquaporin 1 (AQP1)	PTECs-S1, S2, S3	Abcam	AB168387	EPR11588	Rabbit	AF647 (C)	Yes	AQP1, LTL	1	3	NT
Aquaporin 2 (AQP2)	CD-PCs (also GN)	Sigma	HPA04684	PC	Rabbit	UC	NT	AQP2	2	3	NT
Aquaporin 2 (AQP2)	CD-PCs	Abcam	AB199975	EPR21080	Rabbit	UC, AF594, AF647, Cy7 (IH)	Yes	AQP2, AQP1, CALB1, NCC, KRT8, ZO1, THP	2, 3, 12, 25, 26, 27, 30	3	2
Na-glucose cotransporter-2 (SGLT2)	PTECs-S1>S2, no S3	Sigma	HPA041606	PC	Rabbit	UC	NT	AQP1, LTL	19	2	NT
SLC5A12	PTECs-S1, S2>>S3	Santa Cruz	SC-515141	H4	Mouse	UC	NT	AQP1, LTL, LRP2	15, 20	2	1
a-Smooth muscle actin (a-SMA)	VSMCs, MyoFs	Abcam	AB202368	1A4	Mouse	AF594 (C)	Yes	CD31, COL4A12, LAMC1, TNS1, SYNPO	7, 8, 11, 21	1	4
Kerratin-8 (KRT8)	All tubules (not GN)	Novus Bio	NBP2-34267	TS1	Mouse	UC	NT	AQP1, AQP2, THP, CALB1	12, 13	1	NT
Synaptopodin (SYNPO)	Podocyte (cyto/PM)	TF	65194PROGEN	G1D4	Mouse	UC, AF594, AF 647, Cy7 (IH)	Yes*	PODXL, TNS1, WT1, NES, aSMA, CD31, LAMC1, ZO1	11, 16, 17, 22, 23, 28	2, 1	2, 3
Calbindin 1 (CALB1)	DCT2, CNT, C-CDs	Abcam	AB108404 AB208377 AB207528	EPR3478	Rabbit	UC, AF488, AF647 (C)	Yes	NCC, AQP2, THP, KRT8	3, 13	2, 1	2, 3
Tensin (TNS1)	MCs, some VSMCs	Sigma	HPA036089	PC	Rabbit	UC	NT	SYNPO, LAMC1, COL4A12, aSMA, COL4A5, NES	9, 11, 23, 28	1	1
Wilms tumor protein (WT1)	Podocyte (nuc)	Abcam	AB216646	CAN-R9 (IHC)-56-2	Rabbit	UC, AF594	Yes	SYNPO, CD31	22	2	2

Continued

Table 1.— *Continued*

Target	Cell Types	Company	Cat. No.	Clone ID	Species	Conjugate	Conj Test	Antibody Costaining	Supplemental Figs.	Validate Criteria	CyCIF Cycles
Collagen IV a5 (Col IVa5)	GBM, TBM (CD, DCT, CNT), GNcap	Cosmo Bio	SGE-C451 SGE-CFT451	B51	Rat	UC, FITC (C)	Yes**	LAMC1, COL4A1/2, NES, TNS1	9, 10	1	1, 2
Megalin (LRP2)	PTECs-S1>S2, S3	Abcam	AB76969	PC	Rabbit	UC	NT	AQP1, SLC5A12	15	2	NT
Na-K-ATPase a 1, 2, 3, 4 (NaKATPase)	TAL, DCT, CNT> CD >>PTECs	DSHB	A5	A5	Mouse	UC, AF647 (IH)	Yes	THP, NCC, AQP2, AQP1, CALB1	29, 30	1	4
NCC/SLC12A3	DCT	Millipore	AB3553	PC	Rabbit	UC	No	CALB1, AQP2, NaKATPase	3, 29	1	1
Lotus tetragonolobus lectin (LTL)	PTECs-S1, S2, S3, IM-CD-PCs, ICs	Vector Labs	B1325	Lectin	Lectin	Biotin	Yes	AQP1, SLC5A12, SGLT2	1, 19, 20	2	3

Shown are antibodies validated for IF microscopy, including their protein targets, cell types detected, whether directly conjugated antibodies were evaluated, antibody that were used to validate antibody staining characteristics (antibody co-labeling), validation scores (0–3) based on co-labeling studies, whether they were evaluated for CyCIF and, if so, which CyCIF cycles were evaluated for antibody staining. For cell types, see Table 2. C, commercial, IH, in house; NT, not tested; PC, polyclonal antibody; TF, Thermo Fischer; UC, unconjugated. #UMOD/THP antibody (J65429) from Alpha is discontinued. *Fluorophore-conjugated SYNPO antibody stains some tubular nuclei (not unconjugated). **FITC-conjugated COL4A5 antibody is less reliable than the unconjugated antibody. More detailed information is provided in Supplemental Table S1.

Cyclical Immunofluorescence Microscopy

For CyCIF microscopy, after digital images were scanned after a round of staining (CyCIF cycles), slides were returned to humidified chambers at 4°C before initiating de-cover slipping and fluorophore inactivation steps, as previously described (22). Briefly, slides were de-cover slipped by incubating slides in a vertical staining jar in PBS on a gentle plate rocker, washed three times in PBS, and incubated with 0.1 M $NaHCO_3$ (pH 11.2) with 3% hydrogen peroxide (both from Sigma) in water, placed on a transparent plate, and exposed from below to white light [using an LED Cabinet Light (Sears, SPM11582738325)] for 15 min at RT. The process was repeated four times using freshly made solution each time, and then washed three times with PBS. Slides were mounted again in 50% glycerol, coverslipped, and reimaged to confirm that there was fluorophore inactivation before proceeding to the next cycle of IF staining (note that nuclear Hoechst 33342 is not inactivated using this protocol and is used for image registration between scans). Destaining and staining take on average ~2 to 3 h bench work for each cycle, and we complete one cycle every 24 h. This means for four cycle CyCIF, the process will generally take 4 days to complete, as previously described (22). For 3-D CyCIF, 53 sequential sections were obtained from a tissue block, and for a given 3-D series, all the slides underwent staining cycles of CyCIF, as outlined above. CyCIF figure metadata includes information about each of the labeled channel IDs including the antibody, fluorophore, cycle numbers, and comments about the staining and tissue artifacts between cycles (Supplemental Table S2). Supplemental Table S3 also includes information about tissue section quality for the 3-D CyCIF imaging series (Supplemental Table S3).

Digital Image Registration for 2-D Cyclical Immunofluorescence

We used Napari to register images from each of the CyCIF cycles to generate 2-D multiplexed CyCIF images. This can be performed by any laboratory without specialized computational skills by following these step-by-step instructions:

1) Download the latest version of napari from https://github.com/napari/napari/releases/tag/v0.4.19
2) Install napari on your system (available for Windows, MacOS, and Linux)
3) Open the application
4) Click on the "Plugins" > "Install/uninstall plugins…" menu item
5) Search for the "napari-wsireg" plugin (it will appear in the bottom panel) and install it
6) Once installed, it might be necessary to restart napari.
7) Open napari-wsireg by clicking on the "Plugins" > "wsireg2D main" menu item
8) This will open napari-wsireg in the side panel.
9) Clicking on the "Image" button, select your image(s) to register
10) If you are co-registering several MxIF cycles (e.g., 4), you could load each image and then give them names such as cyc1, cyc2, cyc3, and cyc4.
    - Ensure pixel spacing is correctly set for each image. This is typically auto-detected for OME-TIFF or CZI files, but you may need to manually input this if it is not automatically recognized.

- For CyCIF images, set the image type to fluorescence and choose the appropriate channels for co-registration, typically the DAPI channel for cycle co-registration.

11) In the registration setup, identify your cycles with cyc1 as the target modality and cyc2 to cyc4 as the moving modalities
    - Aim for sequential registration to minimize errors, e.g., register cyc4 to cyc3, then cyc3 to cyc2, and finally cyc2 to cyc1
    - Use both rigid and affine models for accurate alignment
    - This approach ensures that each cycle is co-registered with minimized distortion or loss.
12) Once the registration paths have been selected, you must specify the "project name" and the "output directory" where the registration progress and registered images will be saved
    - You can specify advanced options to control whether the preprocessed images should be cached (useful when debugging tricky registration tasks)
    - You can specify whether the "non-transformed" image should be also saved (useful when starting from e.g. CZI image and want to export as OME-TIFF).
13) Click on the "Save config" and export the wsireg configuration file.
14) Click on the "Add to queue" button or the "Run graph" button to start registration.
15) It is also possible to execute wsireg using the command line. Please see https://github.com/NHPatterson/wsireg for more information.

Digital Image Registration for 3-D Cyclical Immunofluorescence

For 3-D image registration, individual CyCIF cycles on the same tissue section were co-registered using the Elastix framework (29), with the DAPI channel utilized for accuracy and precision. To enhance co-registration accuracy, image contrast was adjusted. The "rigid" and "affine" transformation methods were employed for co-registration across the four cycles recorded for each section. We co-registered all cycles to cycle 1. We used cycle 1 as the reference since that cycle typically presented the fewest tissue deformations or changes. Due to the nature of the experiment, minor tissue changes occur between CyCIF cycles. To ensure the best possible co-registration outcomes, cycles are co-registered to their closest neighbor cycle (i.e., cycle 4 is co-registered to cycle 3, cycle 3 to 2, and cycle 2 to 1). However, transformations can be mathematically concatenated, so we also implicitly and automatically co-register cycle 4 to cycle 1, using the calculated transformations of cycle 3 to cycle 2 and cycle 2 to cycle 1 as intermediaries. Since some sections were folded over or damaged between cycles, we defined a binary mask that excluded that part of the tissue in the co-registration step as it yielded better image registration. A similar methodology was applied to obtain the 3-D dataset. Supplemental Table S3 documents instances where tissues were folded, damaged, or CyCIF cycles were out of focus. If a cycle was out of focus or too heavily damaged, it was excluded from the co-registration. In a situation where part of the tissue was folded, or there was a tear in the tissue, a binary mask was drawn excluding that region from co-registration, ensuring that the damaged region does not negatively impact the co-registration outcome. Following individual cycle co-registrations, a VALIS algorithm implementation facilitated the co-registration of remaining tissue sections (30). Initial low-resolution registration involved "rigid," "affine," and "non-linear" transformations, with subsequent refinement at higher spatial resolution using the "non-linear" transformation. Tissues were transformed into a common coordinate space and exported as OME-TIFFs.

Visualizing Digital Immunofluorescence Images

Digital images (including both 2 to 4 + 1 channel and CyCIF registered images) were downloaded into QuPath (v. 0.5.0) and evaluated using the toggle function to switch between channels and identify co-localization and/or proximity of antibody staining to other markers. This can be performed by any laboratory without specialized computational skills by following these step-by-step instructions to evaluate all of our supplemental antibody validation and CyCIF figures:

1) Download most recent version of QuPath which you can find at https://qupath.github.io/. The software is free.
2) Create an empty folder with the name of the project you want to create in QuPath
3) Download the .czi file you want to look at, as well as the associated "supplemental table" excel file that you will find in the OMAP folder. Because of size limitations of Zenodo folders, we had to divide this into four separate folders each with their own Supplemental Table: Part1: Supplemental Figs. S1–S15, Part 2: Supplemental Figs. S16–S30 include all of the antibody validation images; Part 3: Supplemental Figs. S31 and S33 are the two 2D CyCIF images; Part 4: includes two 3-D CyCIF images
4) Open QuPath and click on "create a project"
5) Browse your computer until you find the QuPath project folder and click on it once
6) In QuPath, click on "add images," then click on "choose file" and browse your computer until you find the image you want to analyze
7) Click on "import image." This can take a few second or minutes depending on the size and number of files you import
8) Double click on the image you want to visualize, highlight fluorescence in the pop up, and click on "apply"
9) Ok, now the image is open, and you can go about changing the channels. For this, click on the black and white circle icon. This opens the "brightness and contrast" panel. Each channel is labeled for that figure showing staining with different antibodies, as indicated in the "figures" tab in the excel file you downloaded. If you want to change the color, double click on the channel, and change the color panel. If you want to change the gain and background, click once on the channel, and adjust the channel min and max until you get the image you want. Sometimes antibodies, this has to be adjusted separately for different regions of the kidney.

10) Move around the image by clicking on the cross icon and drag the image with your mouse. Shink the image using your mouse as well.
11) Once you have the colors right for each antibody separately, you can toggle the colors on or off for each of the antibodies using the "brightness and contrast" panel. It is very intuitive.
12) When you are done with that image, double click on the next one. It will ask you if you want to save the settings. I suggest you do so as it will save you time if you come back to that image later.

RESULTS

Antibody Selection

Antibodies that were anticipated to stain cell types or extra cellular matrix (ECM) compartments of interest were initially selected that had evidence on the manufacturer's website and/or in associated publications of target selectivity. Consistent with recently published guidelines on the use of antibodies for research (2, 3), this included evidence from Western blot using overexpressed protein targets, knockout or knockdown cell staining or Western blots, immunoaffinity purification and mass spectrometry, epitope mapping, and/or protein array data showing target selectivity. Preference was given to monoclonal and recombinant monoclonal antibodies, as these provide more reproducible reagents over time (3), but when no other reagents were available, polyclonal antibodies were also selected. We then selected antibodies if they were able to identify images showing staining in the anticipated distribution in the human kidney. After ordering antibodies, we initially performed IF staining at two to three different dilutions, along with immunoglobulin controls, to determine whether the antibody appears to stain the anticipated cell types or ECM compartments, and to establish optimal dilutions, before proceeding to MxIF validation studies.

We evaluated the staining characteristics of 27 different antibodies and one lectin by IF microscopy. These detect 22 protein and glycoprotein targets (Table 1) and can be used in various combinations to identify 18 different cell types and 5 extracellular matrix (ECM) compartments in the human kidney (Table 2). Table 2 also provides abbreviated annotations for the different cell types and ECM compartments identified with this antibody panel. This panel includes 18 monoclonal antibodies, including 5 recombinant rabbit monoclonal and 9 polyclonal antibodies. We also evaluated 16 antibodies that have been directly conjugated with different fluorophores (nine commercial and seven in-house conjugations), all of which gave the anticipated cellular staining after fluorophore conjugation. Direct antibody conjugation allows more highly multiplexed IF analyses with the use of multiple antibodies from the same species on a single tissue section, without concern for cross-reactivity of fluorophore-conjugated secondary antibodies.

Each antibody has been assigned a permanent and unique Research Resource Identification (RRID) in the Antibody Registry (https://www.antibodyregistry.org/) (31). If the same clone is produced by two different manufacturers, they are

Table 2. *Cells and ECM compartments identified using the validated antibody panel*

Cell Types	Abbreviations	Antibody Targets
Podocyte (cytoplasm)	Pod-Cyt	NES, PODXL, SYNPO (low)
Podocyte (plasma membranes)	Pod-PM	ZO1 (high), SYNPO, PODXL
Podocyte (nucleus)	Pod-Nuc	WT1
Mesangial cells	MC	TNS1
All epithelia (except GN epithelium)		KRT8
Proximal tubular epithelial cells (all)	PTECs	AQP1, LTL, KRT8, NaKATPase (low)
Early convoluted PTECs	S1 PTECs	LRP2, SGLT2, SLC5A12, AQP1, LTL, KRT8, NaKATPase (low)
Late convoluted PTECs	S2 PTECs	SLC5A12, SGLT2 (low), LRP2 (low), AQP1, LTL, KRT8, NaKATPase (low)
Straight segment PTECs	S3 PTECs	AQP1, LTL, SLC5A3 (low), KRT8, NaKATPase (low)
Early segment distal convoluted tubule	DCT1	NCC/SLC12A3, ZO1 (low), NaKATPase (high), KRT8
Late segment distal convoluted tubule	DCT2	CALB1, NCC/SLC12A3 (low), ZO1 (low), NaKATPase (high), KRT8
Connecting tubules	CNT	CALB1, AQP2, ZO1 (low), NaKATPase (high), KRT8
Collecting duct (principal cells)	CD-PC	AQP2, KRT8 (highest), NaKATPase (intermediate)
Collecting duct (inner medullary)	CD-IM	LTL, AQP2, KRT8
Collecting duct (intercalated cells)	CD-ICs	LTL
Descending thin limb (loop of Henle)	DLT	AQP1, ZO1 (low), KRT8
Ascending thin limb (loop of Henle)	ATL	KRT8, ZO1 (low)
Thick ascending limb (loop of Henle)	TAL	THP/UMOD, NaKATPase (high), ZO1 (high)
Glomerular endothelial cells	GN-EC	CD31, CD93 (next to COL4A5)
Peritubular endothelial cells	PT-EC	CD31, CD93 (next to COL4A1/2)
Vascular smooth muscle cells	VSMCs	a-SMA, TNS1 (only some arterioles)
Myofibroblasts	MFs	a-SMA
Glomerular basement membrane	GBM	COL4A5, LAMC1
Glomerular capsule	GN-Caps	COL4A1/2, LAMC1, COL4A5 (low)
Tubular basement membrane	TBM	COL4A1/2, LAMC1, COL4A5 (CD, CDT, and CNT only)
Blood vessel walls	BV	LAMC1 (vascular bundles in OM)
Mesangial matrix	MM	COL4A1/2
Peritubular extracellular matrix	PT-ECM	COL4A1/2

Shown are individual and combinations of target antibodies that can be used to define these cell types and extracellular matrix (ECM) compartments. For antibody targets, see Table 1. Low, intermediate, and high refer to staining intensity compared with other cell types that are also detected with this antibody. More detailed information is provided in Supplemental Tables S1 and S2 and can be visualized in Supplemental Figs. S1–S33.

given two different antibody RRIDs. In addition, to establish these antibodies as part of an OMAP panel, we have generated AVRs for each antibody. These include all associated antibody and staining metadata, tissue preparation and staining protocols, and supporting imaging data (https://avr.hubmapconsortium.org/) (20). Each antibody is also linked to the original images used to validate the antibody, with publicly accessible multichannel scanned images of the whole IF-stained human kidney sections in a publicly accessible database (Supplemental Figs. S1–S30, Table 1, and Supplemental Table S1). Access to these images allows investigators to independently evaluate staining throughout the kidney and to optimize thresholds independently in each color channel. As such, they are not dependent on limited views and channel thresholds provided in the static images. Several examples from our antibody panel illustrate the benefits of this: *1*) unlike the AQP1 antibody H4 (RRIDs: AB_626694-unconjugated and AB_3075337-AF647 conjugated) and *Lotus tetragonolobus* lectin (LTL), which stain all proximal tubular epithelial cell (PTEC) segments (Supplemental Fig. S1), the SLC5A12 antibody (RRID: AB_2891092) stains S1 and S2 segment PTECs, which are restricted to the cortex and with much less staining of S3 segment PTECs in the outer stripe of the outer medulla (OSOM) (Supplemental Fig. S20). These differences are not apparent in the renal cortex. *2*) The PECAM/CD31 antibody (RRID: AB_2890260) stains peritubular capillaries clearly but gives a more diffuse staining pattern of glomerular endothelial cells (GN-ECs) than the CD93 antibody (RRID: AB_1846342, Supplemental Fig. S4). However, when background staining in glomeruli is reduced by adjusting image intensity, CD31 staining of GN-EC membranes is comparable to CD93. *3*) The ZO1 polyclonal antibody (RRID: AB_2533938) clearly localizes to podocyte plasma membranes when compared with other, more cytoplasm localized podocyte markers detected using synaptopodin and nNestin antibodies (RRIDs: AB_2335879, and AB_10001441) (Supplemental Fig. S28). However, ZO-1 also stains basolateral plasma membranes in the thick ascending limb (TAL) and collecting duct principal cells (CD-PCs) stained with the THP/UMOD (RRID: AB_2212386) and AQP2 antibodies (RRID: AB_2820249), respectively (Supplemental Figs. S25 and S26). However, basolateral TAL and CD-PC staining is not visible when thresholds are set to detect podocyte staining with the ZO-1 antibody. *4*) The laminin gamma 1/LAMC1 2E8 antibody (RRID: AB_528343) shows more intense staining of glomerular basement membrane (GBM) versus tubular basement membranes (TBMs), but after reducing the image gain so that TBM staining is apparent, it is not possible to discern details of the GBM (Supplemental Figs. S10 and S14).

Antibody Validation

Since our goal was to validate a panel of antibodies that could be used to define the major cell types and extra cellular matrix compartments in human kidney sections, we modified antibody validation criteria that have been used by other laboratories specifically for immunohistochemical validation of tissue samples (5, 27). On this basis, we assigned validation scores (0 to 3) for each antibody using IF to evaluate the localization of antibody staining in relation to other antibody staining patterns as follows: *1*) uncertain (ccore = 0): no staining, incorrect cell type, subcellular localization, or cell state; *2*) approved (score = 1): the correct cell type, subcellular localization, or cell state compared with other antibody data; *3*) supported (score = 2): showing overlapping staining with an antibody for the same cell type, structure, or cell state; and 4) enhanced (score = 3): demonstrating the same staining as an independent antibody against a different epitope on the same protein. Of the 27 antibodies and one lectin tested, one has been discontinued, one stained the wrong cell types in a fluorophore-conjugated form, but not when detected by indirect IF, but the rest met our validation criteria (validation scores $\geq$1) and are recommended for IF on frozen human kidneys. Some were evaluated in multiple studies and given combined scores. For example, LAMC1 2E8 (AB_528343) showed the same staining pattern as LAMC1 antibody D18 (RRID: AB_2281095) (score = 3); overlapping staining with collagen IV α5 (COL4A5) and collagen IV α1/2 (COL4A1/2) (RRIDs: AB_2924380 and AB_2574487, respectively) (score = 2); and when evaluated with the endothelial cell (ECs), CD31 antibody (RRID: AB_2890260) and podocyte markers (podocalyxin antibody, RRID: AB_3065223) showed typical staining of the GBM between the EC and podocyte markers (score = 1) (Supplemental Figs. S10, S14, and S18). These findings only hold true for the application for which these antibodies were evaluated [i.e., IF on frozen human kidneys, as previously described (23, 32)]. The same antibodies may have different staining properties under other conditions. Individual laboratories can then decide on the level of validation required for their applications and whether antibodies need to be reevaluated for their studies.

Cyclical Immunofluorescence Microscopy

We next evaluated 17 of the validated antibodies and one lectin in different combinations for CyCIF to provide a more detailed method to evaluate of tissue segmentation using a larger panel of markers. For example, it is possible to differentiate S1, S2, and S3 segment proximal tubular epithelial cells (PTECs) using combinations antibodies including AQP1 [and/or *Lotus tetroglobinous* lectin (LTL), which stain all PTECs segments, SLC5A12, which stains S1 and S2 > S3 segments, SGLT2 which stains only S1 and S2 segments, and LRP2/megalin, which stains S1 > S2 or S3 PTEC segments] (Table 2). Likewise, it is possible to segment individual glomerular capsules, basement membranes, mesangial matrix, podocytes, mesangial cell, and ECs using a combination of CD31, synaptopodin, WT1, tensin, COL4A1/2, and COL4A5 (or LAMC1) antibodies (Fig. 1 and Table 1). For this, we optimized an established CyCIF protocol (33) for use in our laboratory on frozen human kidney sections (22). Although a limited number of unconjugated antibodies can also be used for CyCIF in early staining/destaining cycles using species-specific fluorophore-conjugated secondary antibodies, this technique is only possible if most antibodies used are directly conjugated with fluorophores. For our CyCIF studies, therefore, we used unconjugated antibodies in early CyCIF cycles when conjugated antibodies for key cell types that we wanted to visualize were not available or had not been properly

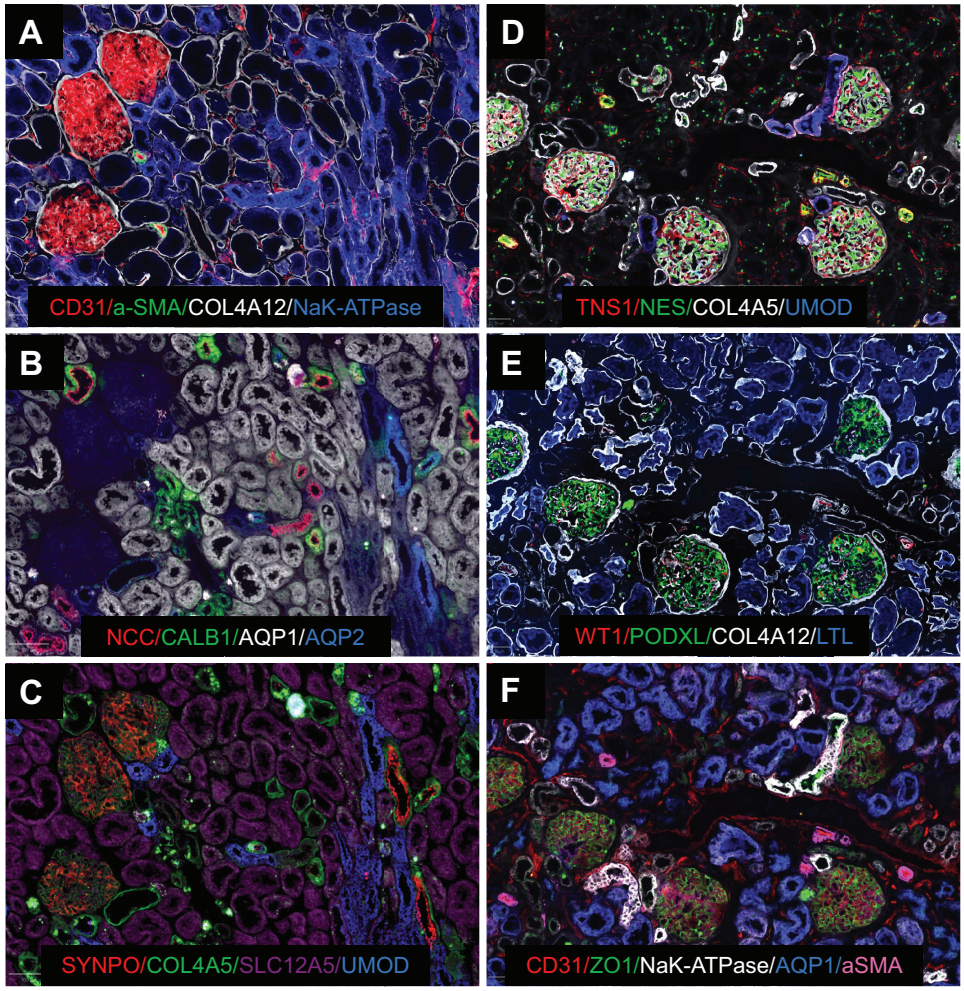

Figure 1. Cyclical immunofluorescence microscopy on normal human kidneys. *A–C*: tubular antibody panel on a kidney mounted in CMC. Scale bars = 100 μm. *D–F*: glomerular antibody panel on a kidney mounted in low melting point gelatin. Scale bars = 50 μm. Antibody targets are indicated under each panel, and each panel was chosen from the merged CyCIF channel images for optimal visualization. Individual channels can be visualized independently in merged multichannel scanned images of the whole kidney sections for both studies in Supplemental Figs. S31 and S33, respectively. Details about the antibodies used and CyCIF cycles for both studies are described in Supplemental Table S2. CMC, carboxymethylcellulose; CyCIF, cyclical immunofluorescence.

validated [e.g., THP/UMOD, WT1, tensin, and NCC/SLC13A3 antibodies (RRIDs: AB_2212386, AB_3065228, AB_10796111, and AB_571116, respectively)]. All other antibodies were directly conjugated with fluorophores either commercially or using our in-house antibody conjugation protocol (28).

These 17 antibodies and one lectin will be the basis for an organ mapping antibody panel (OMAP) for CyCIF microscopy on normal human kidneys (Supplemental Table S2). In the first set of studies, we evaluated a panel of 12 antibodies in four CyCIF cycles designed to optimize tubular cell segmentation (Supplemental Table S2 and Fig. 1, *A–C*). To evaluate the whole tissue block and independently modify threshold values for each of the channels/antibodies indicated in Supplemental Table S2, we have also downloaded the individual CyCIF cycle and 20 channel merged images (12 antibody, 4 nuclear staining, and 4 blank channels) onto Zenodo, an open-source digital image database (Supplemental Fig. S31). These merged images allow the investigator to optimize thresholds and toggle between image channels to provide a more detailed technical validation of CyCIF, and to evaluate of tissue segmentation using multiple complementary markers. Since the destaining protocol used for CyCIF cycles can interfere with subsequent antibody staining, each antibody must be evaluated at a specific CyCIF cycle. As shown in Table 1 and Supplemental Table S2, some antibodies were evaluated at different CyCIF cycles. Antibodies can be used at any cycle less than the cycle tested but need to be reevaluated if they are being used at later cycles. Some antibodies, such as the THP/UMOD antibody (RRID: AB_2212386), work equally well in early (cycle 1, Fig. 1*C*) and later CyCIF cycles (cycle 4, Fig. 1*D*), while others, notably the COL4A5 antibody (RRID: AB_3065220), are sensitive to changes in cycle number. There was intense staining of the GBM and a subset of TBM structures using this COL4A5 antibody in cycle 1 (Fig. 1*D* and Supplemental Fig. S33), but there was a lower signal-to-noise ratio when this antibody was used in cycle 2 (Fig. 1*C* and Supplemental Fig. S31). From these studies, we also noticed bleed-through in AF594 fluorescence between channels. For example, the AQP2 AF594 that was used in cycle 2 of the CyCIF study was still detected in the SYNPO AF594 channel in cycle 3 (compare *B*, blue, with *C*, red, in Fig. 1), indicating there was incomplete quenching of AF594 between CyCIF cycles. To address this, we increased fluorophore quenching from 3 to 5 cycles, and no longer saw bleed-through between AF594 channels (Fig. 1, *D–F*, and Supplemental Figs. S32 and S33).

These studies were performed on frozen sections from tissue blocks mounted in carboxymethyl cellulose (CMC), which is compatible with imaging mass spectrometry methods used by the Vanderbilt Biomolecular Imaging Center in the HuBMAP consortium (23). However, CMC-mounted tissues

are fragile and cannot be reliably cut sequentially across large tissue blocks. To address this, we developed a protocol for the use of low melting point fish gelatin (LMG) (34), as an alternative mounting medium (22). We were able to consistently cut 8-μm sequential sections across large tissue blocks mounted in LMG. To determine whether antibodies perform similarly on CMC- and LMG-mounted tissues, we evaluated nine of the same tubular panel antibodies using for cycles 1, 2, and 4, on an LMG-mounted tissue section (Supplemental Table S2 and Supplemental Fig. S32). Staining characteristics of these antibodies were similar in LMG- and CMC-mounted sections (Supplemental Figs. S31 and S32). Next, we evaluated a panel of antibodies designed to evaluate glomerular and glomerulus-associated structures in sections from the same gelatin-mounted tissue block (Fig. 1, *D–F*, Supplemental Table S2, and Supplemental Fig. S33). This panel included seven new antibodies, LTL lectin, and five of the antibodies used in the tubular segmentation panel, all of which demonstrated the anticipated staining characteristics based on our initial IF validation studies. Further validation of all 17 antibodies and one lectin used for CyCIF studies is provided by comparison with the larger panel of markers. This is summarized in the comments on antibody staining characteristics in the three CyCIF studies we performed that are included in Supplemental Table S2.

Three-Dimensional Cyclical Immunofluorescence Microscopy

Having validated a panel of glomerular and glomerulus-associated antibodies for CyCIF on frozen kidneys mounted in LMG and shown that we could reliably cut sequential sections across large LMG-mounted tissue blocks, we sought to determine whether the same set of antibodies could be used on sequential tissue sections to build a three-dimensional CyCIF composite image of the human kidney. These 3-D images could be used to measure clinically relevant datasets such as glomerular volumes, podocyte cell numbers, tubular segment volumes and cell numbers, and the presence of a tubular glomeruli, which cannot be assessed from simple 2-D images. To address this, we performed CyCIF using the panel of 12 glomerular and glomerulus-associated antibodies and 1 lectin on 53 sequential 8-μm sections taken from the gelatin-mounted tissue block (0.424 mm depth). Following individual cycle co-registrations, VALIS algorithm implementation was used to co-register all of the tissue sections to create a 3-D volume (30). Images were generated using four antibody channels (α-SMA, CD31, Na-K-ATPase, and podocalyxin) from the panel of 13 markers to best visualize 3-D glomerular, tubular (TAL), and vascular segmentation of the human kidney (Fig. 2 and Supplemental Figs. S34 and S35).

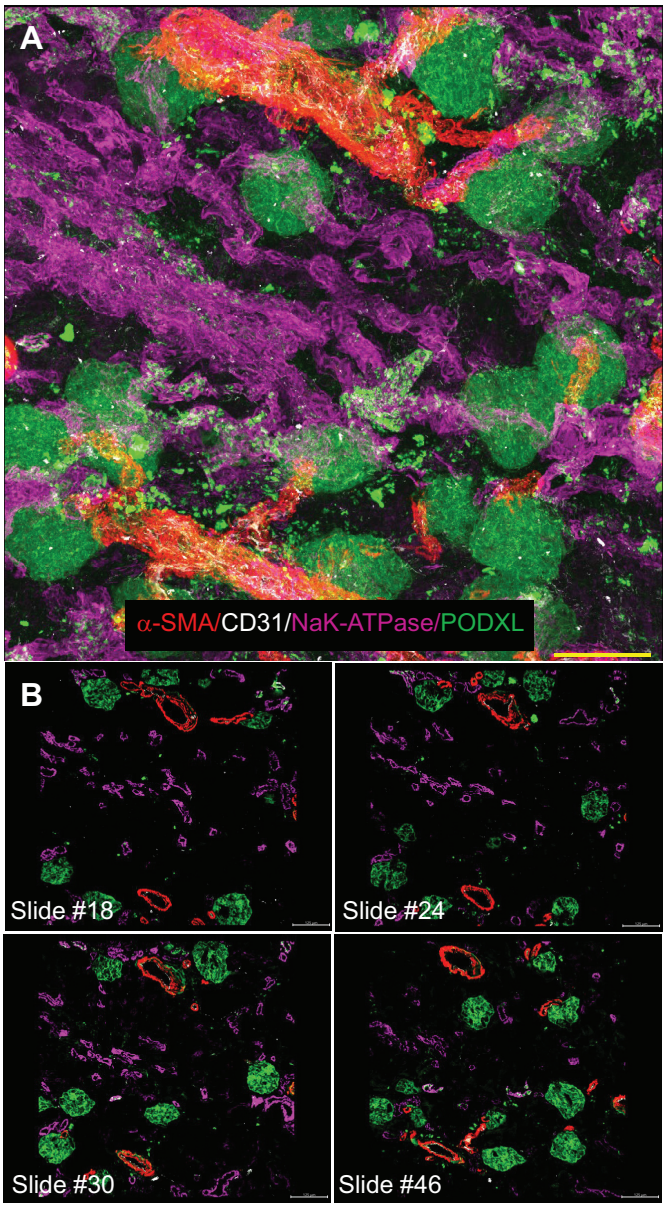

Figure 2. Three-dimensional (3-D) CyCIF microscopy of the human kidney. CyCIF was performed using the glomerular antibody panel on 53 sequential sections obtained from a normal human kidney block mounted in low melting point gelatin. After image registration, 3-D images were generated using 5 antibody channels from the panel of 13 markers for optimal visualization. *A*: 3-D representation showing muscularized vessel branching (a-SMA and CD31 staining) toward individual glomeruli (podocalyxin staining) and tubular structure of the thick ascending limb (UMOD staining). *B*: CyCIF of selected sections from the same series. Scale bars = 125 μm. Details about the antibodies, CyCIF cycles, and tissue sections are described in Supplemental Table S3. Movies through the 3-D series are shown in Supplemental Figs. S34 and S35. CyCIF, cyclical immunofluorescence.

DISCUSSION

In these studies, we describe a standardized approach to validate a panel of 27 antibodies and one lectin for IF microscopy of normal human kidneys. This panel of markers was designed to be used to identify 18 different cell types and 5 ECM compartments in the human kidney and was used to generate a more selective OMAP that includes 17 antibodies and one lectin for CyCIF microscopy of the human kidney. As far as we are aware, this is the most comprehensive and systematic validation of a single antibody panel that can be used to identify the major cell types and ECM compartments in the adult human kidney. Additional kidney-specific CyCIF OMAP antibody panels are currently being validated that will complement this normal tissue OMAP to incorporate markers of cellular injury, proliferation, survival, and signaling that occur in disease states. As of December 2023, there are 13

OMAPs (https://humanatlas.io/omap) covering 11 organs (lymph node, intestines, kidney, spleen, palatine tonsil, full term placenta, eye retina, pancreas, lung, skin, and liver) and 357 antibodies. There are several antibody clones that have been validated independently in different tissues by different research groups, different preservation techniques, and MxIF technologies. Each will have its own AVR. This will allow HuBMAP and the MxIF community to be able to find antibody clones that work universally across many tissues and preservation methods and benefit the global community. More OMAPs are planned for the June 15, 2024, HRA release covering more tissues, preservation methods, and technologies.

A number of guidelines have been published outlining the requirements for antibody validation for different research applications (1–5, 35). Despite this, the lack of standardization in antibody validation remains a major contributor to irreproducibility of research (6). This has been of particular concern with immunohistochemistry since even minor differences in tissue preparation can have significant effects on both nonspecific staining and antibody cross-reactivities (8, 35). Although antibody manufacturers often provide background information that supports the antibody's specificity and selectivity for binding to target proteins, including Western blots using overexpressed protein targets, knockout or knockdown cell-validated staining or Western blots, immunoaffinity purification and mass spectrometry, epitope mapping, and/or protein array data, there is no guarantee that the same antibodies will have target specificity in the more complex milieu of a whole organ tissue section. Indeed, in a recent review on the topic, it was noted that of the ~60,000 antibodies analyzed by the Human Protein Atlas (www.protein.atlas), most of which were validated by Western blot, more than a half did not perform satisfactorily for immunohistochemical applications (3). On this basis, while basic information about antibody specificity should be provided by the manufacturer, the burden of proof for immunohistochemical applications often lies with the investigator. Unless the investigator comes from a laboratory that has a strong focus on antibody validation, cost and time constraints often limit the amount of effort that may seem, at least on the surface, to be a less productive use of their time and money than performing the next hypothesis testing biological experiment. A common theme, however, from all of these guidelines is that the validation criteria should be transparent, and that all of the applicable data and methodologies should made available to the reader for them to independently evaluate. For this reason, we have provided detailed information about tissue preparation, storage, processing, and staining protocols that we have been using and have provided open access to the digital images that we generated using these protocols and antibodies so that the reader is able to independently evaluate their validity.

In addition, the published validation guidelines indicate that validation criteria should be relevant to the application used. In our case, we have used criteria to establish the validity of using our panel of antibodies to stain defined cell types and ECM compartments in the adult human kidney in a reproducible fashion. We therefore consider these antibody "targets" to be the cell types and ECM compartments, rather than individual proteins. This approach is consistent with published guidelines (4), and also speaks to the importance of addressing the specific requirements of the assay being validated, rather than completing a generic template to validate all antibodies for all possible applications in the same way. For example, for our application, we do not necessarily have to independently show that our antibodies bind to exactly the same protein molecules in these tissue sections as was specified in the manufacturer's datasheets [e.g., using Proximity Ligations Assays to show that two antibodies bind to the same protein by demonstrating a signal that only appears when both antibodies bind the same molecule in a tissue section (36)]. This information can be inferred from the anticipated cellular and ECM distribution of antibody staining pattern based on published data, for example from studies using different antibodies, or orthologous methods such as in situ hybridization, and/or single cell RNA sequencing etc., which define the anticipated cellular expression of the target protein/gene. For our purposes, therefore, to show that the antibodies bind to the anticipated cellular or ECM targets, we have performed co-labeling studies with other antibodies that determine, with different degrees of certainty (i.e., approved, supported, or enhanced), that the antibodies are only staining the anticipated cell types or ECM structures. In this way, we provide a practical approach for antibody validation that meets our specific experimental needs and no more.

Since the methods we use for CyCIF microscopy do not require specialized instrumentation, and image registration required to assemble CyCIF images can be performed by any laboratory without specialized computational skills by following the step-by-step instructions provided in this manuscript, they are accessible to any laboratory with access to a fluorescence microscope with a digital image scanner, enabling spatial cellular phenotyping and the discovery of cellular neighborhoods in normal and disease states. In addition, CyCIF microscopy makes it possible to perform highly multiplexed IF microscopy of whole slide images, which is an advantage over some of the other MxIF imaging techniques that are only applicable to limited fields of view. This enables a broader view of cell distributions across large anatomical regions and organ systems, allowing a better chance of capturing localized regions of dysfunction in diseased tissues. This ability to perform multiplexed imaging without specialized reagents or instrumentation also opens the door to integration with other molecular imaging modalities such as spatial transcriptomics and imaging mass spectrometry (IMS), enabling the discovery of molecular markers of specific cell types and how those molecular profiles are altered in diseased tissues. Untargeted molecular imaging data provide deeper molecular content but without a direct link to specific cell types or anatomical features, which is necessary to fully describe drivers of disease. Integrating MxIF data with technologies such as spatial transcriptomics and imaging mass spectrometry allows cellular information to be layered on top of molecular profiles. This is underscored when analysis at scale by means of machine learning driven analysis is considered. An example of this is the automated biomarker candidate discovery previously described in Tideman et al. (37) Here, the search for molecular species that are differentially expressed between biological structures and states was approached in an automated manner by bringing together high-dimensional IMS measurements with microscopy-supplied spatial delineations

of tissue structures and cell types of interest, using machine learning methodology to automatically identify biomarker candidates and estimate their relevance to recognizing the biological class of interest.

Currently, machine learning approaches have primarily been demonstrated in 2-D scenarios. However, since biological (and pathological) processes are, in reality, playing out in a 3-D context, there is a concern that such processes are suboptimally sampled or described in 2-D experiments, which could lead to missed observations. It is therefore pressing to generalize multimodal analyses to make them inherently 3-D-aware. The availability of machine learning approaches to integrate and mine such massively high-dimensional datasets holds enormous potential to reveal new insights into specific diseases. As an initial step toward this goal, our studies have shown that CyCIF microscopy on sequential sections can be effectively co-registered using mathematical algorithms to generate 3-D volumes. Future studies will use validated OMAPs to provide three-dimensional human kidney structure delineations, segmentations, and annotations, prerequisites to unlocking some of the added spatial specificity that 3-D datasets can bring. Other approaches, such as tissue cytometry, which allows multiplexed analysis with a limited number of antibodies in thick tissue sections (50 to 100 μm) in 3-D, provide an alternative approach (26, 38, 39). However, unlike CyCIF, this methodology does not lend itself scale, allowing analysis across larger volumes of tissue that would allow integration with other highly multiplexed lipid, metabolite, protein, RNA, and DNA datasets that are obtained on sequential sections cut through the body of the kidney.

DATA AVAILABILITY

Additional data not provided in the Supplemental Data will be made available upon reasonable request.

SUPPLEMENTAL DATA

Supplemental figures and tables have been uploaded in the following datasets:

Antibody validation for IF microscopy of human kidneys (Supplemental Table S1 and Supplemental Figs. S1–S15): https://doi.org/10.5281/zenodo.10407947.

Antibody validation for IF microscopy of human kidneys (Supplemental Table S1 and Supplemental Figs. S16–S30):https://doi.org/10.5281/zenodo.10440321.

Antibody validation for cyclical IF of human kidneys (Supplemental Table S2 and Supplemental Figs. S31 and S33): https://doi.org/10.5281/zenodo.10445539.

Antibody validation for cyclical IF of human kidneys (Supplemental Table S2 and Supplemental Fig. S32): https://doi.org/10.5281/zenodo.10445552.

3-D cyclical IF microscopy of the human midney (Supplemental Table S3 and Supplemental Figs. S34 and S35): https://doi.org/10.5281/zenodo.10447489.

ACKNOWLEDGMENTS

We thank the patients who consented to have kidney samples removed at nephrectomy used for research and the Vanderbilt Cooperative Human Tissue Network for obtaining patient consent, deidentifying and collecting tissues from the operating rooms, and separating tumor-associated normal tissue from surgical pathology specimens after nephrectomy. The authors also thank Diane Saunders (Department of Medicine at Vanderbilt University Medical Center, Nashville, TN) for help creating an OMAP community for all of the supplemental data on Zenodo and for providing figures for the graphical abstract.

GRANTS

This work was supported by the National Institutes of Health (NIH) Common Fund and National Institute of Diabetes and Digestive and Kidney Diseases Grants U54DK134302 and U01DK133766 (to J.M.S., R.V., and M.D.C.), by the NIH Common Fund and National Eye Institute Grant U54EY032442 (to J.M.S. and R.V.), by National Institute on Aging Grant R01AG078803 (to J.M.S. and R.V.), and by NIH Common Fund Human Biomolecular Atlas Program Grant OT2OD026671 (to E.M.Q.). This work was also supported in part by Grants 2021-240339 and 2022-309518 (to L.G.M. and R.V.) from the Chan Zuckerberg Initiative DAF, an advised fund of the Silicon Valley Community Foundation.

DISCLAIMERS

The content is solely the responsibility of the authors and does not necessarily represent the official views of the National Institutes of Health.

DISCLOSURES

No conflicts of interest, financial or otherwise, are declared by the authors.

AUTHOR CONTRIBUTIONS

E.M.Q., R.V.d.P., and M.P.d.C. conceived and designed research; M.B., K.A.C., J.L.A., D.M.A., E.P., and M.F. performed experiments; M.B., L.G.M., R.V.d.P., and M.P.d.C. analyzed data; RL.G.M., J.M.S., V.d.P., and M.P.d.C. interpreted results of experiments; L.G.M., K.A.C., and M.P.d.C. prepared figures; M.P.d.C. drafted manuscript; M.B., L.G.M., E.M.Q., J.M.S., R.V.d.P., and M.P.d.C. edited and revised manuscript; M.P.d.C. approved final version of manuscript.

REFERENCES

1. **Bordeaux J**, **Welsh A**, **Agarwal S**, **Killiam E**, **Baquero M**, **Hanna J**, **Anagnostou V**, **Rimm D.** Antibody validation. *Biotechniques* 48: 197–209, 2010 [Erratum in Biotechniques 48: 351, 2010]. doi:10.2144/000113382.
2. **Uhlen M**, **Bandrowski A**, **Carr S**, **Edwards A**, **Ellenberg J**, **Lundberg E**, **Rimm DL**, **Rodriguez H**, **Hiltke T**, **Snyder M**, **Yamamoto T.** A proposal for validation of antibodies. *Nat Methods* 13: 823–827, 2016. doi:10.1038/nmeth.3995.
3. **Taussig MJ**, **Fonseca C**, **Trimmer JS.** Antibody validation: a view from the mountains. *N Biotechnol* 45: 1–8, 2018. doi:10.1016/j.nbt.2018.08.002.
4. **Weller MG.** Ten basic rules of antibody validation. *Anal Chem Insights* 13: 1177390118757462, 2018. doi:10.1177/1177390118757462.
5. **MacNeil T**, **Vathiotis IA**, **Martinez-Morilla S**, **Yaghoobi V**, **Zugazagoitia J**, **Liu Y**, **Rimm DL.** Antibody validation for protein expression on tissue slides: a protocol for immunohistochemistry. *Biotechniques* 69: 460–468, 2020. doi:10.2144/btn-2020-0095.
6. **Roy AL**, **Wilder EL**, **Anderson JM.** Validation of antibodies: lessons learned from the common fund protein capture reagents program. *Sci Adv* 7: eabl7148, 2021. doi:10.1126/sciadv.abl7148.
7. **Baker M.** A spellchecker for statistics. *Nature* 540: 151–152, 2016. doi:10.1038/540151a.
8. **Bolognesi MM**, **Mascadri F**, **Furia L**, **Faretta M**, **Bosisio FM**, **Cattoretti G.** Antibodies validated for routinely processed tissues

stain frozen sections unpredictably. *Biotechniques* 70: 137–148, 2021. doi:10.2144/btn-2020-0149.

9. **Börner K**, **Bueckle A**, **Herr BW**, **Cross LE**, **Quardokus EM**, **Record EG**, **Ju Y**, **Silverstein JC**, **Browne KM**, **Jain S**, **Wasserfall CH**, **Jorgensen ML**, **Spraggins JM**, **Patterson NH**, **Weber GM.** Tissue registration and exploration user interfaces in support of a human reference atlas. *Commun Biol* 5: 1369, 2022. doi:10.1038/s42003-022-03644-x.
10. **Hansen J**, **Sealfon R**, **Menon R**, **Eadon MT**, **Lake BB**, **Steck B**, **et al**. A reference tissue atlas for the human kidney. *Sci Adv* 8: eabn4965, 2022. doi:10.1126/sciadv.abn4965.
11. **Chen S**, **Zhu B**, **Huang S**, **Hickey JW**, **Lin KZ**, **Snyder M**, **Greenleaf WJ**, **Nolan GP**, **Zhang NR**, **Ma Z.** Integration of spatial and single-cell data across modalities with weak linkage. *Nat Biotechnol*. In press. doi:10.1101/2023.01.12.523851.
12. **Alfaro JA**, **Bohländer P**, **Dai M**, **Filius M**, **Howard CJ**, **van Kooten XF**, **et al.** The emerging landscape of single-molecule protein sequencing technologies. *Nat Methods* 18: 604–617, 2021. doi:10.1038/s41592-021-01143-1.
13. **Black S**, **Phillips D**, **Hickey JW**, **Kennedy-Darling J**, **Venkataraaman VG**, **Samusik N**, **Goltsev Y**, **Schürch CM**, **Nolan GP.** CODEX multiplexed tissue imaging with DNA-conjugated antibodies. *Nat Protoc* 16: 3802–3835, 2021. doi:10.1038/s41596-021-00556-8.
14. **Neumann EK**, **Patterson NH**, **Rivera ES**, **Allen JL**, **Brewer M**, **deCaestecker MP**, **Caprioli RM**, **Fogo AB**, **Spraggins JM.** Highly multiplexed immunofluorescence of the human kidney using co-detection by indexing. *Kidney Int* 101: 137–143, 2022. doi:10.1016/j.kint.2021.08.033.
15. **Lin JR**, **Fallahi-Sichani M**, **Sorger PK.** Highly multiplexed imaging of single cells using a high-throughput cyclic immunofluorescence method. *Nat Commun* 6: 8390, 2015. doi:10.1038/ncomms9390.
16. **Radtke AJ**, **Chu CJ**, **Yaniv Z**, **Yao L**, **Marr J**, **Beuschel RT**, **Ichise H**, **Gola A**, **Kabat J**, **Lowekamp B**, **Speranza E**, **Croteau J**, **Thakur N**, **Jonigk D**, **Davis JL**, **Hernandez JM**, **Germain RN.** IBEX: an iterative immunolabeling and chemical bleaching method for high-content imaging of diverse tissues. *Nat Protoc* 17: 378–401, 2022. doi:10.1038/s41596-021-00644-9.
17. **Giesen C**, **Wang HA**, **Schapiro D**, **Zivanovic N**, **Jacobs A**, **Hattendorf B**, **Schüffler PJ**, **Grolimund D**, **Buhmann JM**, **Brandt S**, **Varga Z**, **Wild PJ**, **Günther D**, **Bodenmiller B.** Highly multiplexed imaging of tumor tissues with subcellular resolution by mass cytometry. *Nat Methods* 11: 417–422, 2014. doi:10.1038/nmeth.2869.
18. **Jain S**, **Pei L**, **Spraggins JM**, **Angelo M**, **Carson JP**, **Gehlenborg N**, **Ginty F**, **Gonçalves JP**, **Hagood JS**, **Hickey JW**, **Kelleher NL**, **Laurent LC**, **Lin S**, **Lin Y**, **Liu H**, **Naba A**, **Nakayasu ES**, **Qian W-J**, **Radtke A**, **Robson P**, **Stockwell BR**, **Van de Plas R**, **Vlachos IS**, **Zhou M**, **Börner K**, **Snyder MP.** Advances and prospects for the Human BioMolecular Atlas Program (HuBMAP). *Nat Cell Biol* 25: 1089–1100, 2023 [Erratum in *Nat Cell Biol* 2024]. doi:10.1038/s41556-023-01194-w.
19. **HUBMAP-Consortium.** The human body at cellular resolution: the NIH Human Biomolecular Atlas Program. *Nature* 574: 187–192, 2019. doi:10.1038/s41586-019-1629-x.
20. **Quardokus EM**, **Saunders DC**, **McDonough E**, **Hickey JW**, **Werlein C**, **Surrette C**, **et al.** Organ Mapping Antibody Panels: a community resource for standardized multiplexed tissue imaging. *Nat Methods* 20: 1174–1178, 2023. doi:10.1038/s41592-023-01846-7.
21. **Börner K**, **Teichmann SA**, **Quardokus EM**, **Gee JC**, **Browne K**, **Osumi-Sutherland D**, **et al**. Anatomical structures, cell types and biomarkers of the Human Reference Atlas. *Nat Cell Biol* 23: 1117–1128, 2021. doi:10.1038/s41556-021-00788-6.
22. **Brewer M**, **McDonough L**, **Zhu Y**, **Neuman E**, **Gutierrez D**, **Spraggins J**, **de Caestecker MP.** *Protocols.io. Multiplex Cyclical Immunofluorescence on Fresh Frozen Tissue-V3 V.3* [Online]. doi:10.17504/protocols.io.81wgb1m3yvpk/v3.
23. **Neuman E**, **Allen J**, **Brewer M**, **Anderson D**, **de Caestecker M**, **Gutierrez D**, **Spraggins J.** *Protocols.io. VU Biomolecular Multimodal Imaging Center (BIOMIC) Kidney Characterization Pipeline for Tissues Collected Through the Cooperative Human Tissue Network (CHTN) V.4* [Online]. doi:10.17504/protocols.io.bfskjncw.
24. **Kruse ARS**, **Spraggins JM.** Uncovering molecular heterogeneity in the kidney with spatially targeted mass spectrometry. *Front Physiol* 13: 837773, 2022. doi:10.3389/fphys.2022.837773.
25. **Neumann EK**, **Patterson NH**, **Tideman LEM**, **Migas LG**, **Colley ME**, **Farrow MA**, **Allen JL**, **Rivera ES**, **Romer CE**, **Yang H**, **Brewer M**, **Sharman K**, **Harris RC**, **Fogo AB**, **Gutierrez DB**, **de Caestecker MP**, **Caprioli RM**, **de Plas RV**, **Spraggins JM.** A multiscale lipid and cellular atlas of the human kidney (Preprint). *bioRxiv*. In press. doi:10.1101/2022.04.07.487155.
26. **El-Achkar TM**, **Eadon MT**, **Kretzler M**, **Himmelfarb J**; **Kidney Precision Medicine Project.** Precision medicine in nephrology: an integrative framework of multidimensional data in the kidney precision medicine project. *Am J Kidney Dis* 83: 402–410, 2024. doi:10.1053/j.ajkd.2023.08.015.
27. **O'Hurley G**, **Sjostedt E**, **Rahman A**, **Li B**, **Kampf C**, **Ponten F**, **Gallagher WM**, **Lindskog C.** Garbage in, garbage out: a critical evaluation of strategies used for validation of immunohistochemical biomarkers. *Mol Oncol* 8: 783–798, 2014. doi:10.1016/j.molonc.2014.03.008.
28. **Brewer MZY**, **Gitierrez D**, **Spraggins J**, **de Caestecker MP.** *Protocols.io. Antibody Purification and Labeling V.1* [Online]. doi:10.17504/protocols.io.667hhhn.
29. **Klein S**, **Staring M**, **Murphy K**, **Viergever MA**, **Pluim JP.** elastix: a toolbox for intensity-based medical image registration. *IEEE Trans Med Imaging* 29: 196–205, 2010. doi:10.1109/TMI.2009.2035616.
30. **Gatenbee CD**, **Baker A-M**, **Prabhakaran S**, **Swinyard O**, **Slebos RJC**, **Mandal G**, **Mulholland E**, **Andor N**, **Marusyk A**, **Leedham S**, **Conejo-Garcia JR**, **Chung CH**, **Robertson-Tessi M**, **Graham TA**, **Anderson ARA.** Virtual alignment of pathology image series for multi-gigapixel whole slide images. *Nat Commun* 14: 4502, 2023. doi:10.1038/s41467-023-40218-9.
31. **Bandrowski AE**, **Martone ME.** RRIDs: a simple step toward improving reproducibility through rigor and transparency of experimental methods. *Neuron* 90: 434–436, 2016. doi:10.1016/j.neuron.2016.04.030.
32. **Brewer M**, **Zhu Y**, **Clouthier K**, **Spraggins J**, **de Caestecker M.** *Protocols.io. Immunofluorescence on Fresh Frozen Kidney Tissue - Validation of Antibodies V.1* [Online]. doi:10.17504/protocols.io.5jyl8pwwdg2w/v1.
33. **Gerdes MJ**, **Sevinsky CJ**, **Sood A**, **Adak S**, **Bello MO**, **Bordwell A**, **Can A**, **Corwin A**, **Dinn S**, **Filkins RJ**, **Hollman D**, **Kamath V**, **Kaanumalle S**, **Kenny K**, **Larsen M**, **Lazare M**, **Li Q**, **Lowes C**, **McCulloch CC**, **McDonough E**, **Montalto MC**, **Pang Z**, **Rittscher J**, **Santamaria-Pang A**, **Sarachan BD**, **Seel ML**, **Seppo A**, **Shaikh K**, **Sui Y**, **Zhang J**, **Ginty F.** Highly multiplexed single-cell analysis of formalin-fixed, paraffin-embedded cancer tissue. *Proc Natl Acad Sci USA* 110: 11982–11987, 2013. doi:10.1073/pnas.1300136110.
34. **Ushida K**, **Asai N**, **Uchiyama K**, **Enomoto A**, **Takahashi M.** Development of a method to preliminarily embed tissue samples using low melting temperature fish gelatin before sectioning: a technical note. *Pathol Int* 68: 241–245, 2018. doi:10.1111/pin.12652.
35. **Brooks HL**, **de Castro Brás LE**, **Brunt KR**, **Sylvester MA**, **Parvatiyar MS**, **Sirish P**, **Bansal SS**, **Sule R**, **Eadie AL**, **Knepper MA**, **Fenton RA**, **Lindsey ML**, **DeLeon-Pennell KY**, **Gomes AV.** Guidelines on antibody use in physiology research. *Am J Physiol Renal Physiol* 326: F511–F533, 2024. doi:10.1152/ajprenal.00347.2023.
36. **Lindskog C**, **Backman M**, **Zieba A**, **Asplund A**, **Uhlen M**, **Landegren U**, **Ponten F.** Proximity ligation assay as a tool for antibody validation in human tissues. *J Histochem Cytochem* 68: 515–529, 2020. doi:10.1369/0022155420936384.
37. **Tideman LEM**, **Migas LG**, **Djambazova KV**, **Patterson NH**, **Caprioli RM**, **Spraggins JM**, **Van de Plas R.** Automated biomarker candidate discovery in imaging mass spectrometry data through spatially localized Shapley additive explanations. *Anal Chim Acta* 1177: 338522, 2021. doi:10.1016/j.aca.2021.338522.
38. **Sabo AR**, **Winfree S**, **El-Achkar TM.** Defining protein expression in the kidney at large scale: from antibody validation to cytometry analysis. *Am J Physiol Renal Physiol* 324: F135–F137, 2023. doi:10.1152/ajprenal.00262.2022.
39. **Ferkowicz MJ**, **Winfree S**, **Sabo AR**, **Kamocka MM**, **Khochare S**, **Barwinska D**, **Eadon MT**, **Cheng YH**, **Phillips CL**, **Sutton TA**, **Kelly KJ**, **Dagher PC**, **El-Achkar TM**, **Dunn KW**; **Kidney Precision Medicine Project.** Large-scale, three-dimensional tissue cytometry of the human kidney: a complete and accessible pipeline. *Lab Invest* 101: 661–676, 2021. doi:10.1038/s41374-020-00518-w.